

## Threshold-cusp explanation for $X$ and $Z_{cs}$ in $B^+ \rightarrow J/\psi\phi K^+$

S.X. NAKAMURA<sup>(1)</sup>(\*) and X. LUO<sup>(2)</sup>

<sup>(1)</sup> *Institute of Frontier and Interdisciplinary Science, Shandong University - Qingdao, China*

<sup>(2)</sup> *School of Physics and Optoelectronics Engineering, Anhui University - Hefei, China*

**Summary.** — Several  $X$  and  $Z_{cs}$  exotic hadrons were claimed in the LHCb's amplitude analysis on  $B^+ \rightarrow J/\psi\phi K^+$ . The data shows that all the peaks and also dips in the spectra are located at thresholds of seemingly relevant meson-meson channels. While the LHCb analysis fitted the peaks with Breit-Wigner resonances, threshold kinematical cusps might be the cause of such structures. We thus analyze the LHCb data considering the threshold cusps. Our model is simultaneously fitted to  $J/\psi\phi$ ,  $J/\psi K^+$ , and  $K^+\phi$  invariant mass distributions. The threshold cusps fit well all the  $X$ ,  $Z_{cs}$ , and dip structures. Our analysis indicates that spin-parity of the  $X(4274)$  and  $X(4500)$  structures are  $0^-$  and  $1^-$ , respectively. This is different from the LHCb's spin-parity assignments ( $1^+$  and  $0^+$ ). The number of fitting parameters can be significantly reduced by considering the relevant threshold cusps. Our analysis shows that  $D_s^{(*)}\bar{D}^*$  scattering lengths are consistent with zero. This disfavors an explanation of  $Z_{cs}(4000)$  and  $Z_{cs}(4220)$  as  $D_s^{(*)}\bar{D}^*$  molecules, which is consistent with lattice QCD via the SU(3) relation.

### 1. – Introduction

The LHCb's six-dimensional amplitude analysis for  $B^+ \rightarrow J/\psi\phi K^+$  found several  $X$  and  $Z_{cs}$  exotic states that are different from the conventional  $q\bar{q}$  [1, 2, 3]. Those appearing as bumps in the  $J/\psi\phi$  invariant mass ( $M_{J/\psi\phi}$ ) distribution are  $X(4140)$  and  $X(4274)$  with  $J^P = 1^+$ , and  $X(4500)$  and  $X(4700)$  with  $J^P = 0^+$  ( $J$ : spin,  $P$ : parity). Also,  $Z_{cs}(4000)^+$  and  $Z_{cs}(4220)^+$  with  $J^P = 1^+$  appear as bumps in the  $M_{J/\psi K^+}$  distribution. The mass, width, and  $J^P$  are primarily important for studying the nature and structures of the exotic hadrons. However, due to assumptions and simplifications, amplitude analysis results are sometimes not unique nor model-independent.

A basic assumption in the LHCb's amplitude analysis is that all the bumps are caused by resonances that can be well simulated by the Breit-Wigner form. However, the  $X$  bumps are located at  $D_s^*\bar{D}_s^{(*)}$ ,  $D_{sJ}^{(*)}\bar{D}_s^{(*)}$ , and  $\psi'\phi$  thresholds, and the  $Z_{cs}$  bumps at

---

(\*) satoshi@sdu.edu.cn

$D_s^{(*)}\bar{D}^*$  thresholds. There are also dips at other thresholds. Since resonancelike and dip structures might have been generated by threshold cusps, the LHCb's assumption of using the Breit-Wigner amplitudes should be viewed with caution. The assumption would also influence the  $J^P$  assignments. The LHCb's  $J^P$  assignments might change if threshold cusps at the peaks and dips are taken into account in fitting the data. It seems important to conduct an independent amplitude analysis for the same process with due consideration of the threshold cusps, and compare with the LHCb's results.

The nature of the  $Z_{cs}(4000)$  and  $Z_{cs}(4220)$  has been a controversial issue. The BE-SIII collaboration observed a similar structure,  $Z_{cs}(3985)$ , in  $e^+e^- \rightarrow K^+(D_s^-D^{*0} + D_s^{*-}D^0)$  [4]. Their masses are similar:  $4003 \pm 6_{-14}^{+4}$  MeV for  $Z_{cs}(4000)$  and  $3982.5_{-2.6}^{+1.8} \pm 2.1$  MeV for  $Z_{cs}(3985)$ . However, their widths are rather different:  $131 \pm 15 \pm 26$  MeV for  $Z_{cs}(4000)$  and  $12.8_{-4.4}^{+5.3} \pm 3.0$  MeV for  $Z_{cs}(3985)$ . Several proposals have been made to understand whether  $Z_{cs}(3985)$  and  $Z_{cs}(4000)$  are the same or different, and whether they are  $cu\bar{c}s$  tetraquark state or  $D_s^{(*)}\bar{D}^{(*)}$  molecules. It is also possible that a virtual pole enhances the  $D_s\bar{D}^*$  threshold cusp to generate the  $Z_{cs}(3985)$  and  $Z_{cs}(4000)$  structures.  $Z_{cs}(3985/4000)$  and  $Z_c(3900)$  [5] may be SU(3) partners. The existence of a narrow  $Z_c(3900)$  state is disfavored by Lattice QCD (LQCD) calculations, implying that  $Z_c(3900)$  may be a kinematical effect. Via the SU(3) relation, the LQCD is not in favor of the existence of a narrow  $Z_{cs}(3985/4000)$  state.

In this work, we develop a reaction model for  $B^+ \rightarrow J/\psi\phi K^+$  (<sup>1</sup>). Then, the model is fitted to the LHCb data of the  $J/\psi\phi$ ,  $J/\psi K^+$ , and  $K^+\phi$  invariant mass distributions simultaneously. We show that ordinary  $s$ -wave threshold cusps from one-loop diagrams in Fig. 1 can fit all the peaks and dips in the  $M_{J/\psi\phi}$  and  $M_{J/\psi K^+}$  distributions, and no virtual poles near the thresholds are necessary. Our model indicates that the  $X(4274)$  and  $X(4500)$  structures are from the  $D_{s0}^*(2317)^+D_s^-$  and  $D_{s1}(2536)^+D_s^-$  threshold cusps that have  $J^P = 0^-$  and  $1^-$ , respectively. This is different from the LHCb's  $J^P$  assignments ( $J^P = 1^+$  and  $0^+$ ), which would originate from quite different mechanisms in the models. Possible advantages of our model over the LHCb's model will be pointed out. Furthermore, we examine whether the LHCb data favors the  $D_s^{(*)}\bar{D}^*$  molecule interpretation of  $Z_{cs}(4000)$  and  $Z_{cs}(4220)$ . Our analysis will show that the data requires the  $D_s^{(*)}\bar{D}^*$  scattering lengths to be consistent with zero within our model. Thus the molecule interpretation is disfavored. This is actually consistent with the above-mentioned LQCD implication.

## 2. – Model

For describing the structures in the  $M_{J/\psi\phi}$  and  $M_{J/\psi K^+}$  distributions of  $B^+ \rightarrow J/\psi\phi K^+$  with threshold cusps, one-loop mechanisms of Figs. 1(a-c) are considered.  $K_J^*$  resonance mechanisms of Fig. 1(d) are also considered and they would shape the  $M_{K^+\phi}$  distribution. In the one-loop mechanisms of Fig. 1(a),  $s$ -wave pairs of  $D_{s0}^*(2317)^+D_s^-(0^-)$ ,  $D_{s0}^*(2317)^+D_s^{*-}(1^-)$ ,  $D_{s1}(2536)^+D_s^-(1^-)$ , and  $D_{s1}(2536)^+D_s^{*-}(0^-)$  are included;  $J^P$  is indicated in the parenthesis. In one-loop mechanisms of Fig. 1(b),  $s$ -wave pairs of  $D_s^{*+}D_s^-(1^+)$ ,  $D_s^{*+}D_s^{*-}(0^+)$ ,  $\psi'\phi(0^+)$ , and  $\psi'\phi(1^+)$  are included. In Fig. 1(c),  $s$ -wave pairs of  $D_s^+\bar{D}^{*0}(1^+)$  and  $D_s^{*+}\bar{D}^{*0}(1^+)$  are included in the one-loop. Several  $K_J^*$  resonance mechanisms in Breit-Wigner forms are considered in Fig. 1(d).

---

(<sup>1</sup>) See Ref. [6] for the full account of this work.

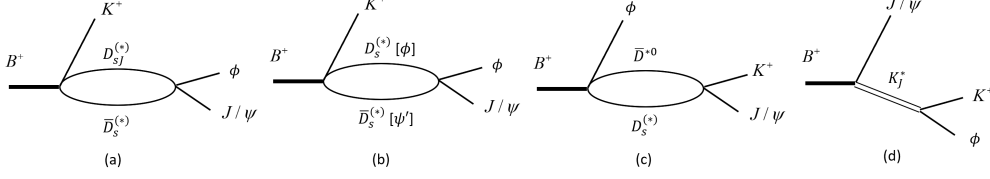


Fig. 1. – Diagrams for  $B^+ \rightarrow J/\psi\phi K^+$  considered in this work. (a) one-loop of  $D_{sJ}^{(*)+} D_s^{(*)-}$  ( $0^-, 1^-$ ); (b) one-loop of  $D_s^{(*)+} D_s^{(*)-}$  and  $\psi'\phi$  ( $0^+, 1^+$ ); (c) one-loop of  $D_s^{(*)+} \bar{D}^{*0}$  ( $1^+$ ); (d)  $K_J$  ( $K, K^*, K_1, K_2$ ) resonances.  $D_{sJ}^{(*)}$  refers to  $D_{s0}^*$  (2317) and  $D_{s1}$  (2536), and  $\psi'$  is  $\psi(2S)$ . Figures taken from Ref. [6]. Copyright (2021) APS.

An amplitude formula for Fig. 1(c) with a  $D_s^+ \bar{D}^{*0}(1^+)$  pair is given below as a representative case. The energy, width, three-momentum and polarization vector of a particle  $x$  are denoted by  $E_x$ ,  $\Gamma_x$ ,  $\vec{p}_x$  and  $\vec{\varepsilon}_x$ , respectively. We refer to the PDG [7] for the particle masses and widths. The amplitudes includes a  $B^+ \rightarrow D_s^+ \bar{D}^{*0} \phi$  vertex, which is parity-conserving (pc), and a  $D_s^+ \bar{D}^{*0} \rightarrow J/\psi K^+$  interaction. Their matrix elements are

$$(1) \quad c_{D_s \bar{D}^{*0}(1^+)}^{\text{pc}} \vec{\varepsilon}_{\bar{D}^{*0}} \cdot \vec{\varepsilon}_\phi F_{D_s \bar{D}^{*0} \phi, B}^{00}, \quad c_{\psi K, D_s \bar{D}^{*0}}^{1^+} \vec{\varepsilon}_{\bar{D}^{*0}} \cdot \vec{\varepsilon}_\psi f_{\psi K}^0 f_{D_s \bar{D}^{*0}}^0,$$

respectively, where  $c_{D_s \bar{D}^{*0}(1^+)}^{\text{pc}}$  and  $c_{\psi K, D_s \bar{D}^{*0}}^{1^+}$  are coupling constants. We have introduced dipole form factors denoted by  $F_{ij k, l}^{LL'}$  and  $f_{ij}^L$  where a common cutoff of  $\Lambda = 1$  GeV is used in all form factors. Combining the above matrix elements, the amplitude for Fig. 1(c) with  $D_s^+ \bar{D}^{*0}(1^+)$  is given as

$$(2) \quad A_{\bar{D}^{*0} D_s(1^+)}^{1\text{L,pc}} = c_{\psi K, D_s \bar{D}^{*0}}^{1^+} c_{D_s \bar{D}^{*0}(1^+)}^{\text{pc}} \vec{\varepsilon}_\psi \cdot \vec{\varepsilon}_\phi \int d^3 p_{D_s} \frac{f_{\psi K}^0 f_{D_s \bar{D}^{*0}}^0 F_{D_s \bar{D}^{*0} \phi, B}^{00}}{M_{\psi K} - E_{D_s} - E_{\bar{D}^{*0}} + i\varepsilon}.$$

The product of coupling constants ( $c_{\psi K, D_s \bar{D}^{*0}}^{1^+} c_{D_s \bar{D}^{*0}(1^+)}^{\text{pc}}$ ), which is a complex overall factor, is determined by fitting the LHCb data. In our default fit, we use 16 mechanisms in total, giving  $2 \times 16 - 3 = 29$  fitting parameters. Since the absolute normalization of the full amplitude and overall phases of the parity-conserving and -violating full amplitudes are arbitrary, we subtracted 3 from the number of the fitting parameters.

There might be virtual or bound states near the  $D_s^{(*)+} \bar{D}^{*0}$  thresholds, and they could enhance the threshold cusps from Eq. (2). This effect can be implemented in our model by describing the  $D_s^{(*)+} \bar{D}^{*0} \rightarrow J/\psi K^+$  transition with a single-channel  $D_s^{(*)+} \bar{D}^{*0}$  scattering, and a perturbative  $D_s^{(*)+} \bar{D}^{*0} \rightarrow J/\psi K^+$  transition follows. Our  $D_s^{(*)+} \bar{D}^{*0}$  interaction potential is

$$(3) \quad v_\alpha(p', p) = f_\alpha^0(p') h_\alpha f_\alpha^0(p),$$

where an interaction channel is labeled by  $\alpha$  and the coupling constant is  $h_\alpha$ . The rescattering effect on the  $Z_{CS}$  structures are not included in our default fit, but it will be studied separately.

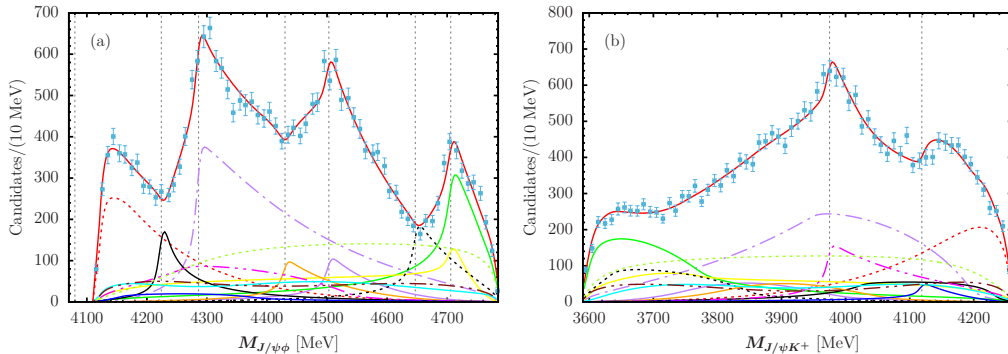


Fig. 2. – (a)  $J/\psi\phi$  and (b)  $J/\psi K^+$  invariant mass distributions for  $B^+ \rightarrow J/\psi\phi K^+$ . The data are from LHCb [3]. Our default fit is shown by the red solid curves. Each loop contribution of Fig. 1(a-c) is shown such as  $D_s^{*+}D_s^-(1^+)$  by red-dashed,  $D_s^{*+}D_s^{*-}(0^+)$  by black-solid,  $D_{s0}^*(2317)^+D_s^-(0^-)$  by purple-dash-dotted,  $D_{s0}^*(2317)^+D_s^{*-}(1^-)$  by orange-solid,  $D_{s1}(2536)^+D_s^-(1^-)$  by purple-solid,  $D_{s1}(2536)^+D_s^{*-}(0^-)$  by black-dashed,  $\psi'\phi(0^+)$  by green-solid,  $\psi'\phi(1^+)$  by yellow-solid,  $D_s^+\bar{D}^{*0}(1^+)$  by magenta-dash-two-dotted, and  $D_s^{*+}\bar{D}^{*0}(1^+)$  by blue-solid. Also, each contribution from Fig. 1(d) is shown:  $K^*$  by cyan-solid,  $K_1$  by green-dashed, and  $K_2$  by brown-dash-two-dotted. The dotted vertical lines indicate threshold locations. From left to right,  $D_s^+\bar{D}_s$ ,  $D_s^*\bar{D}_s$ ,  $D_{s0}^*(2317)\bar{D}_s$ ,  $D_{s0}^*(2317)\bar{D}_s^*$ ,  $D_{s1}(2536)\bar{D}_s$ ,  $D_{s1}(2536)\bar{D}_s^*$ , and  $\psi'\phi$  thresholds for the panel (a), and  $D_s^+\bar{D}^{*0}$  and  $D_s^{*+}\bar{D}^{*0}$  thresholds for the panel (b). Figures taken from Ref. [6]. Copyright (2021) APS.

### 3. – Results and discussions

The LHCb data for  $B^+ \rightarrow J/\psi\phi K^+$  such as the  $M_{J/\psi\phi}$ ,  $M_{J/\psi K^+}$ , and  $M_{K^+\phi}$  distributions are simultaneously fitted with the above-described model, and the fit result is shown in Fig. 2. The LHCb data are well fitted by our default model. The fit quality can be quantified by  $\chi^2/\text{ndf} = 1.77$  where ndf is the number of degrees of freedom (the number of bins subtracted by the number of fitting parameters).

The peaks in the  $M_{J/\psi\phi}$  distribution are well fitted by the threshold cusps such as: the  $X(4140)$  peak by the  $D_s^{*+}D_s^-(1^+)$  threshold cusp [red dashed curve],  $X(4274)$  by  $D_{s0}^*(2317)^+D_s^-(0^-)$  [purple dash-dotted],  $X(4500)$  by  $D_{s1}(2536)^+D_s^-(1^-)$  [purple solid], and  $X(4700/4685)$  by  $\psi'\phi(0^+/1^+)$  [green solid/yellow solid]. Also, the three dips are generated by the corresponding threshold cusps located at  $D_s^{*+}D_s^{*-}(0^+)$  [black solid],  $D_{s0}^*(2317)^+D_s^{*-}(1^-)$  [orange solid], and  $D_{s1}(2536)^+D_s^{*-}(0^-)$  [black dashed] thresholds.

For the  $M_{J/\psi K^+}$  distribution, the  $Z_{cs}(4000)$ -like peak is well described by the  $D_s^+\bar{D}^{*0}(1^+)$  threshold cusp shown by the magenta dash-two-dotted curve. The  $Z_{cs}(4220)$ -like structure is also formed by our model. However, it is not from a resonance but from the  $D_s^{*+}\bar{D}^{*0}(1^+)$  threshold cusp [blue solid] appearing as a dip and the shrinking phase-space near the kinematical endpoint.

There are several qualitative differences between our and LHCb's analysis results. Our model describes all  $X$  and  $Z_{cs}$  structures with the threshold cusps, while the LHCb's model uses the Breit-Wigner-type resonances. Our model also has threshold cusps for the dips in the  $M_{J/\psi\phi}$  spectrum. On the other hand, the LHCb's model uses interferences to generate the dips. Probably due to the differences in the mechanisms, the  $J^P$  assignments to the  $X(4274)$  and  $X(4500)$  peaks are also different:  $0^-$  for  $X(4274)$  and  $1^-$  for  $X(4500)$

in our model, but  $1^+$  for  $X(4274)$  and  $0^+$  for  $X(4500)$  in the LHCb's.

The number of fitting parameters ( $N_p$ ) is also rather different between our and LHCb's models. Our default model has  $N_p = 29$  to fit the  $M_{J/\psi\phi}$ ,  $M_{J/\psi K^+}$ , and  $M_{K^+\phi}$  distributions, while the LHCb's amplitude model has  $N_p = 144$  to fit the six-dimensional distribution. Since the LHCb's model is fitted to the richer information,  $N_p$  should be larger to some extent. Nevertheless, this alone does not seem to fully explain the larger  $N_p$  in the LHCb's model. A possible explanation for the large  $N_p$  is that relevant mechanisms are missed in the LHCb's model, and this needs to be compensated for by including many other mechanisms and complicated interferences.

In the default fit, the  $Z_{cs}$ -like structures in the  $M_{J/\psi K^+}$  distribution are well described by the threshold cusps and no nearby poles are necessary. Does the LHCb data allow a molecule (pole) scenario for the  $Z_{cs}$  structures? We address this question by varying the fitting parameters involved in Fig. 1(c), and also  $D_s^+\bar{D}^{*0}$  and  $D_s^{*+}\bar{D}^{*0}$  interaction strengths  $h_\alpha$  in Eq. (3);  $h_\alpha$  for the  $D_s^+\bar{D}^{*0}$  interaction and that for  $D_s^{*+}\bar{D}^{*0}$  can take different values. Then we obtain the allowed regions for the two  $h_\alpha$  values. We obtain the regions for the  $D_s^+\bar{D}^{*0}$  interaction strength as  $-0.33 < h_\alpha < 0.93$ , corresponding to the scattering length of  $-0.12 < a(\text{fm}) < 0.06$ . This indicates that a virtual pole exists at 93 MeV below the  $D_s^+\bar{D}^{*0}$  threshold or deeper. Similarly, we obtain the regions for the  $D_s^{*+}\bar{D}^{*0}$  interaction strength as  $-0.17 < h_\alpha < 2.02$ , corresponding to  $-0.21 < a(\text{fm}) < 0.03$ , and a virtual pole exists at 103 MeV below the threshold or deeper. This result indicates that the LHCb data does not favorably support the interpretation that the  $Z_{cs}$  structures are  $D_s^{(*)+}\bar{D}^{*0}$  molecules.

The previous LQCD calculations for the  $J^{PC} = 1^{+-} D^*\bar{D}$  scattering indicated that the interaction is weak, and that the scattering would not form a bound or narrow resonance corresponding to  $Z_c(3900)$ . Via the SU(3) relation, the LQCD results implies that the  $Z_{cs}(4000)$  structure in the LHCb data would not be due to a  $D_s^+\bar{D}^{*0}$  molecule. Our default model as well as the analysis result in the previous paragraph are consistent with this LQCD finding. Phenomenologically, however, the  $Z_c(3900)$  [5] and  $Z_{cs}(3985)$  [4] peak structures in the data have not been well explained by a non-pole scenario. Experimental, phenomenological, and LQCD studies are more needed to draw a consistent picture for  $Z_{c(s)}$ .

\* \* \*

SXN is supported by National Natural Science Foundation of China (NSFC) under contracts U2032103. XL is supported by the National Natural Science Foundation of China under Grant No. 12205002.

## REFERENCES

- [1] Aaij R. et al. (LHCb Collaboration), *Phys. Rev. Lett.* **118** (2017) 022003.
- [2] Aaij R. et al. (LHCb Collaboration), *Phys. Rev. D* **95** (2017) 012002.
- [3] Aaij R. et al. (LHCb Collaboration), *Phys. Rev. Lett.* **127** (2021) 082001.
- [4] Ablikim M. et al. (BESIII Collaboration), *Phys. Rev. Lett.* **126** (2021) 102001.
- [5] Ablikim M. et al. (BESIII Collaboration), *Phys. Rev. Lett.* **119** (2017) 072001.
- [6] Luo X. and Nakamura S.X., *Phys. Rev. D* **107** (2023) L011504.
- [7] Zyla P.A. et al. (Particle Data Group), *Prog. Theor. Exp. Phys.* **2020** (2020) 083C01.